Heliocentric Trajectory Analysis of Sun-pointing Smart Dust with Electrochromic Control

Giovanni Mengali and Alessandro A. Quarta *

Department of Civil and Industrial Engineering, University of Pisa, I-56122 Pisa, Italy

Abstract

A smart dust is a micro spacecraft, with a characteristic side length on the order of a few millimeters, whose surface is coated with electrochromic material. Its orbital dynamics is controlled by exploiting the differential force due to the solar radiation pressure, which is obtained by modulating the reflectivity coefficient of the electrochromic material within a range of admissible values. A significant thrust level can be reached due to the high values of area-to-mass ratio of such a spacecraft configuration. Assuming that the smart dust is designed to achieve a passive Sun-pointing attitude, the propulsive acceleration due to the solar radiation pressure lies along the Sun-spacecraft direction. The aim of this paper is to study the smart dust heliocentric dynamics in order to find a closed form, analytical solution of its trajectory when the reflectivity coefficient of the electrochromic material can assume two values only. The problem is addressed by introducing a suitable transformation that regularizes the spacecraft motion and translates the smart-dust dynamics into that of a linear harmonic oscillator with unitary frequency, whose forcing input is a boxcar function. The solution is found using the Laplace transform method, and afterwards the problem is generalized by accounting for the degradation of the electrochromic material due to its exposition to the solar radiation. Three spacecraft configurations, corresponding to low, medium and high performance smart dusts, are finally used to quantify the potentialities of these advanced devices in an interplanetary mission scenario.

Key words: Smart dust, Spacecraft-on-a-chip, Electrochromic control, Radial thrust

Nomenclature

A	=	smart dust effective reflective area, [cm^2]
$\mathcal{A}, \mathcal{B}$	=	dimensionless auxiliary function, see Eqs. (17)-(18)
$\boldsymbol{a}_P$	=	acceleration due to radiation pressure, [$\mathrm{mm/s}^2$]
a_c	=	spacecraft characteristic acceleration, [$\mathrm{mm/s}^2$]
$\mathcal{E}$	=	specific mechanical energy of osculating orbit, [$\mathrm{km}^2/\mathrm{s}^2$]
H	=	Heaviside step function
m	=	smart dust total mass, [g]
O	=	Sun's center-of-mass
p	=	osculating orbit's semilatus rectum, [au]
P	=	solar radiation pressure, [Pa]
$\boldsymbol{r}$	=	position vector, with $r = \|\boldsymbol{r}\|$, [au]
s	=	complex variable
T	=	degradation half-life, [year]
$\mathcal{T}(O; r, \theta)$	=	polar heliocentric reference frame
$\boldsymbol{v}$	=	inertial velocity vector, [km/s]
β	=	lightness number, see Eq. (2)
ϵ	=	degradation parameter, [year^{-1}]
η	=	reflectivity coefficient
θ	=	polar angle, [deg]
$\mu_\odot$	=	Sun's gravitational parameter, [$\mathrm{km}^3/\mathrm{s}^2$]
ρ	=	dimensionless auxiliary variable, see Eq. (6)

* Corresponding author.
Email addresses: g.mengali@ing.unipi.it (Giovanni Mengali), a.quarta@ing.unipi.it (Alessandro A. Quarta).

ϕ = apse line rotation angle, [deg]

Subscripts

0 = initial, parking orbit

$\oplus$ = one astronomical unit

esc = escape

fin = final orbit

max = maximum

min = minimum

Superscripts

$\cdot$ = time derivative

$'$ = derivative w.r.t. θ

$\sim$ = dimensionless variable

1 Introduction

Technological advances in the miniaturization process of components used for space applications make potentially possible the realization of micro spacecraft, characterized by dimensions comparable to that of a common microchip, that is, on the order of some centimeters or even some millimeters (Atchison and Peck, 2010). These devices have an area-to-mass ratio much greater than that of typical spacecraft, with the consequence that their orbital dynamics is highly influenced, and in some cases dominated, by a number of effects (including solar radia-

tion pressure, atmospheric drag, electrostatic forces etc.) that are usually thought of as simple perturbative forces for conventional space vehicles (Colombo and McInnes, 2011; Colombo et al., 2012).

Micro spacecraft represent a very attractive option for future space missions (especially in a planetary mission scenario) due their unique characteristics, such as the low manufacturing costs, the cheap launch costs related to the possibility of deployment from a CubeSat or as piggy back on more conventional spacecraft, the high spatial coverage offered by the potential large number of objects that can be launched and operated simultaneously (Colombo and McInnes, 2012). To maximize their effectiveness, these devices should be equipped with suitable means, capable of modifying their orbital dynamics. An interesting solution is to cover the micro spacecraft surface with electrochromic material (Lücking et al., 2012, 2010; Colombo et al., 2013), which is able to change its optical properties on application of a voltage. Accordingly, and accounting for their microscopic dimensions, such devices are also termed Smart Dusts (SDs) (Colombo and McInnes, 2011).

The orbital dynamics of SDs have been studied by Colombo and McInnes (2011, 2012), and Colombo et al. (2012) by investigating the combined effects caused by the solar radiation pressure, atmospheric drag and Earth's oblateness in a planetary mission scenario. In this context, SDs with electrochromic coatings have also been suggested as a solution to extend the mission lifetime. In particular, a simple control law with a bang-bang control, similar to the time-optimal control of a linear oscillator, is discussed by Lücking et al. (2012) and Colombo et al. (2013), while Lücking et al. (2010) propose an artificial potential field control algorithm that uses a reflectivity change twice per orbit.

The use of micro spacecraft, and so of SDs, is potentially a feasible option also within a heliocentric mission scenario. In this respect the original paper by Atchison and Peck (2010) contains some interesting ideas on possible practical application of those small spacecraft.

For example, Atchison and Peck (2010) point out that a micro spacecraft could be used to maintain suitable non-Keplerian (or even displaced) orbits in the vicinity of Earth, or to reach a Solar System escape condition. Note, however, that the use of either a single or multiple micro spacecraft for a deep space mission implies that the characteristic distances between the SDs are at least an order of magnitude greater than those necessary within a planetocentric range. This may represent a serious problem due to the limited capabilities of data transmission (in terms of maximum allowable range) between two SDs or one SD and the Earth (or the mothership used for orbital deployment) .

In this paper the heliocentric orbital dynamics and control of a SD is investigated from a new viewpoint, aimed at obtaining analytical expressions for its deep space trajectory. To this end the SD is designed to be passively Sun-pointing, while its orbital dynamics exploits the propulsive effect of the solar radiation pressure to produce a purely (outward) radial thrust, i.e. a propulsive thrust aligned with the Sun-spacecraft direction. The analysis is conducted under the assumption that the reflectivity coefficient of the electrochromic material, which covers the SD surface, can take two values only. The SD dynamics is first described using an extension of the Bürdet-Ferrándiz regularization method. As a result, the SD heliocentric trajectory can be calculated analytically for a generic control law in the form of a boxcar function. Finally the degradation effect of the material is accounted for by means of a simplified model in which the SD reflectivity reduces with time according to an exponential decreasing law. A closed form solution to the SD trajectory is found even in this more complex case.

2 Smart dust heliocentric dynamics

Consider a SD spacecraft, characterized by a mass m and an effective area A, the latter being equal to the projection of the surface exposed to the solar radiation onto a plane perpendicular to the Sun-spacecraft line. The SD surface is assumed to be covered by electrochromic material,

which is able to change, when operated by a suitable voltage, its reflectivity coefficient in the range $\eta \in \{\eta_{\min}, \eta_{\max}\}$. In particular, as long as the electrochromic system is turned off, the reflectivity coefficient takes a value equal to $\eta_{\min} \geq 1$, where the liming case $\eta_{\min} = 1$ corresponds to a completely absorptive surface. On the other side, when the electrochromic system is switched on, the reflectivity coefficient takes its maximum admissible value $\eta_{\max} \leq 2$, where $\eta_{\max} = 2$ corresponds to a completely reflective surface. In this sense, the heliocentric orbital dynamics of a SD spacecraft is consistent with the dynamics of a photonic solar sail with reflection control devices (Aliasi et al., 2013; Gong and Li, 2015, 2014a,b; Mu et al., 2015).

In this paper the SD geometry is chosen such that the external force due to the solar radiation pressure is always aligned with the Sun-SD line. This is possible, for example, using a SD with a spherical shape, or by means of a suitable passive pointing system similar to that described by Atchison and Peck (2010). In the case of a spherical SD with radius R, the effective area turns out to be $A = \pi R^2$. If, instead, the SD shape resembles a Sun-facing square chip (Atchison and Peck, 2010) of side ℓ, its effective area is simply $A = \ell^2$.

Under the assumption of a propulsive force due to the incoming photons directed along the Sun-SD line, the propulsive acceleration $\boldsymbol{a}_P$, which varies as the inverse square distance from the Sun, can be written as

$$\boldsymbol{a}_P = \frac{\eta\, P_\oplus\, A\, r_\oplus^2}{m\, r^3}\, \boldsymbol{r} \tag{1}$$

where $P_\oplus = 4.56\,\mathrm{N/km^2}$ is the solar radiation pressure at a distance $r_\oplus \triangleq 1\,\mathrm{au}$ from the Sun, $\boldsymbol{r}$ is the SD position vector and $r = \|\boldsymbol{r}\|$. In analogy with the usual convention adopted for a photonic solar sail (McInnes, 1999), the propulsive acceleration is more conveniently rewritten with the introduction of the lightness number β, defined as the ratio between the modulus of the propulsive acceleration and the modulus of the local gravitational acceleration at a distance

$r = r_\oplus$, or

$$\beta \triangleq \frac{\eta\, P_\oplus\, A\, r_\oplus^2}{m\, \mu_\odot} \tag{2}$$

where $\mu_\odot$ is the Sun's gravitational parameter. Accordingly, the equivalent form of Eq. (1) is

$$\boldsymbol{a}_P = \frac{\mu_\odot}{r^3}\, \beta\, \boldsymbol{r} \tag{3}$$

In this paper the reflectivity coefficient is assumed to take two possible values only, either $\eta_{\min}$ or $\eta_{\max}$, depending on the electrochromic materials. These two values, when substituted into Eq. (2), provide the corresponding minimum ($\beta_{\min}$) or maximum ($\beta_{\max}$) value of the lightness number.

As far as photonic solar sails are concerned, such a methodology of trajectory control is usually referred to as "β-control", and its effectiveness has been studied in several missions scenarios, including orbital transfers (McInnes, 2003; Yamakawa, 2006; Quarta and Mengali, 2011) as well as for generation and control of artificial equilibrium points (Biggs and McInnes, 2010; Aliasi et al., 2012, 2014). The main drawback of such a control means is due to the purely radial nature of the propulsive acceleration, which is therefore unable to change the spacecraft orbital plane, nor the SD angular momentum. As a matter of fact the heliocentric SD motion turns out to be two-dimensional and belonging to the orbital plane of the osculating orbit at the initial time instant $t_0 \triangleq 0$. Assuming that during the launch phase a certain number of SDs are all placed inside the same container, such an osculating orbit can be thought of as the heliocentric parking orbit of the container after the escape phase from Earth. Since all external forces acting on the SD are in the Sun-spacecraft (radial) direction, it turns out that the semilatus rectum of the osculating orbit is a constant of motion.

The time history of the control variable β is often chosen as the output of an optimization process, aimed at minimizing (or maximizing) a suitable scalar performance index. For example, the control law necessary for reaching an osculating orbit of given (feasible) characteristics, could be obtained with a minor adaptation of the technique developed by Quarta and Mengali

(2009) when the propulsion system was a Sun-facing photonic solar sail. However, this paper is not intended for obtaining the optimal performance of a SD with electrochromic material. Rather, its aim is to get the heliocentric trajectory of a SD in an analytical form, as a function of the control variable β.

To begin, introduce a polar reference frame $\mathcal{T}(O; r, \theta)$, with its origin at the Sun's center of mass O, in which the polar angle θ is measured anticlockwise from the Sun-SD direction at time t_0, see Fig. 1. Bearing in mind Eqs. (2)-(3), the SD dynamics can be described by the differential equations

$$\dot{\theta} = \frac{\sqrt{\mu_\odot \, p_0}}{r^2} \tag{4}$$

$$\ddot{r} = \frac{\mu_\odot}{r^2} \left(\frac{p_0}{r} + \beta - 1 \right) \tag{5}$$

where p_0 is the semilatus rectum of the osculating orbit at the initial time t_0, and β, which depends on time, can assume one of the two previous values, i.e. either $\beta = \beta_{\min}$ or $\beta = \beta_{\max}$. Note that the circumferential velocity component of the SD is equal to $\sqrt{\mu_\odot \, p_0}/r$.

For the sake of convenience, the polar angle is now chosen as the independent variable in place of the time t. The following transformation is therefore introduced:

$$\rho \triangleq 1 - \beta_{\min} - \frac{p_0}{r} \tag{6}$$

from which, taking into account Eq. (4), the equivalent form of the radial velocity and acceleration are

$$\dot{r} = \rho' \sqrt{\frac{\mu_\odot}{p_0}} \qquad , \qquad \ddot{r} = \frac{\mu_\odot}{p_0^2} \, \rho'' \, (1 - \beta_{\min} - \rho)^2 \tag{7}$$

where the prime symbol denotes a derivative taken with respect to the polar angle θ. The transformation (6) is a variant of that used by McInnes (2003) and Yamakawa (2006) for describing the dynamics of a Sun-facing photonic solar sail. More generally, Eq. (6) is a direct extension of the Bürdet-Ferrándiz regularization (Bürdet, 1969; Ferrándiz, 1987) of the two-

body motion. In particular, the Bürdet-Ferrándiz regularization allows the nonlinear Keplerian dynamics around a primary to be reduced to the dynamics of a harmonic oscillator with a suitable restoring force. Details on the derivation of the reduced equations of motion along with an interesting analysis of the practical implications of the regularization process, are thoroughly discussed in the paper by Fukushima (2007).

Actually, this same transformation has been used by the authors to analyze the trajectory of a spacecraft subjected to a radial propulsive acceleration of constant modulus (Quarta and Mengali, 2012), or to a series of radial and tangential impulses (Quarta and Mengali, 2010), as well as to study the heliocentric motion of an electric solar wind sail (Quarta and Mengali, 2015).

When Eqs. (6)-(7) are substituted into Eq. (5), the result is

$$\rho'' = \frac{p_0}{r} + \beta - 1 \tag{8}$$

which can be more conveniently written as

$$\rho'' + \rho = \Delta\beta \tag{9}$$

where $\Delta\beta \in \{0,\, \Delta\beta_{\max}\}$, with $\Delta\beta_{\max} \triangleq (\beta_{\max} - \beta_{\min})$. In other terms, the variation of ρ (and so the variation of the Sun-SD distance) with the polar angle is described by the differential equation of a single degree of freedom linear harmonic oscillator with unitary frequency, with the following two initial conditions (calculated at a polar angle $\theta = 0$)

$$\rho_0 \triangleq \rho(0) = 1 - \beta_{\min} - \frac{p_0}{r_0} \qquad , \qquad \rho_0' \triangleq \rho'(0) = \frac{\dot{r}_0}{\sqrt{\mu_\odot / p_0}} \tag{10}$$

where $r_0 \triangleq r(t_0)$ and $\dot{r}_0 \triangleq \dot{r}(t_0)$ are the initial Sun-SD distance and radial velocity, respectively. The two initial conditions can also be expressed as a function of the eccentricity e_0 and true anomaly ν_0 (calculated at t_0) along the initial osculating orbit, that is

$$\rho_0 = -\beta_{\min} - e_0 \cos\nu_0 \qquad , \qquad \rho_0' = e_0 \sin\nu_0 \tag{11}$$

From the last equations it turns out that $\rho(0)$ is in general different from zero, except the special case in which $e_0 \cos\nu_0 = -\beta_{\min}$, whereas $\rho'(0)$ is zero only when the osculating orbit is circular or the SD initial position coincides with either the orbit's perihelion or its aphelion.

Equation (9) is formally similar to that found by McInnes (2003) for a Sun-facing photonic solar sail. However in that case the lightness number was assumed to vary with continuity in the range $[\beta_{\min}, \beta_{\max}]$ as a function of the polar angle θ. In this paper, instead, the β-control (that is, the function $\Delta\beta = \Delta\beta(\theta)$) is a piecewise constant function as is shown in Fig. 2. In particular, the figure schematizes N working cycles of the electrochromic material. The generic i-th cycle starts by switching the electrochromic system on (i.e. $\eta = \eta_{\max}$ or $\beta = \beta_{\max}$) when the SD polar angle is θ_{on_i} and ends by switching it off (i.e. $\eta = \eta_{\min}$ or $\beta = \beta_{\min}$) at an angle $\theta_{\mathrm{off}_i} > \theta_{\mathrm{on}_i}$, with $i \in \mathbb{N}$ and $i \leq N$.

We are now in a position to solve the problem of calculating the heliocentric SD trajectory using the discrete version of the β-control law, thus extending the results discussed by McInnes (2003). This is the subject of next section.

3 Heliocentric trajectory in polar form

The SD trajectory can be obtained by solving the Cauchy problem constituted by Eqs. (9)-(10). To this end, it is useful to first assume $N = 1$. In this case there is a single working cycle of the electrochromic material, which is turned on at $\theta = \theta_{\mathrm{on}} \geq 0$ and then turned off at $\theta > \theta_{\mathrm{off}}$. Accordingly, $\Delta\beta = \Delta\beta_{\max}$ as long as $\theta \in [\theta_{\mathrm{on}}, \theta_{\mathrm{off}}]$, otherwise $\Delta\beta = 0$, see Fig. 2. In other terms $\Delta\beta = \Delta\beta(\theta)$ is a boxcar function, which can be written as

$$\Delta\beta(\theta) = \Delta\beta_{\max}\ [H(\theta - \theta_{\mathrm{on}}) - H(\theta - \theta_{\mathrm{off}})] \tag{12}$$

where $H(x)$ is the Heaviside step function, defined as $H(x) = 0$ if $x < 0$, and $H(x) = 1$ if $x \geq 0$. The Cauchy problem can be solved through the Laplace transform method. When Eq. (12) is substituted into (9), the Laplace transform is applied to both sides of the differential equation, and the initial conditions (10) are taken into account, the result is

$$\rho(s) = \frac{s\,\rho_0 + \rho_0'}{s^2+1} + \frac{\Delta\beta_{\max}\,[\exp(-\theta_{\text{on}}\,s) - \exp(-\theta_{\text{off}}\,s)]}{s\,(s^2+1)} \tag{13}$$

where s is the complex variable. The inverse Laplace transform of Eq. (13) is

$$\rho(\theta) = \rho_0\,\cos\theta + \rho_0'\,\sin\theta + \Delta\beta_{\max}\,\{H(\theta-\theta_{\text{on}})\,[1-\cos(\theta-\theta_{\text{on}})] - H(\theta-\theta_{\text{off}})\,[1-\cos(\theta-\theta_{\text{off}})]\} \tag{14}$$

The trajectory equation is therefore simply obtained by solving Eq. (6) for r, viz.

$$r(\theta) = \frac{p_0}{1-\beta_{\min}-\rho(\theta)} \tag{15}$$

where $\rho(\theta)$ is given by Eq. (14). From Eq. (15), the SD distance from the Sun can be calculated, in an analytical and exact form, as a function of the polar angle θ. The trajectory consists of a sequence of conic arcs joined, in terms of position and velocity, at the points where the reflectivity of the electrochromic material is changed, that is when $\theta = \{\theta_{\text{on}},\,\theta_{\text{off}}\}$. The latter conclusion can be better verified by considering the final trajectory, that is, the trajectory tracked by the SD when $\theta > \theta_{\text{off}}$. In that case $H(\theta-\theta_{\text{on}}) = H(\theta-\theta_{\text{off}}) = 1$, and Eq. (15) reduces to

$$r_{\text{fin}}(\theta) = \frac{p_0}{1-\beta_{\min}-\mathcal{A}\,\cos\theta-\mathcal{B}\,\sin\theta} \equiv \frac{p_0}{1-\beta_{\min}-\sqrt{\mathcal{A}^2+\mathcal{B}^2}\,\cos\left(\theta-\phi_{\text{fin}}\right)} \tag{16}$$

where

$$\mathcal{A} \triangleq \rho_0 - \Delta\beta_{\max}\,(\cos\theta_{\text{on}} - \cos\theta_{\text{off}}) \tag{17}$$

$$\mathcal{B} \triangleq \rho_0' - \Delta\beta_{\max}\,(\sin\theta_{\text{on}} - \sin\theta_{\text{off}}) \tag{18}$$

and

$$\phi_{\text{fin}} \triangleq \arctan\left(\frac{\mathcal{B}}{\mathcal{A}}\right) \tag{19}$$

Note that Eq. (16) actually corresponds to the polar equation of a conic, since it can be rewritten as

$$r_{\text{fin}}(\theta) = \frac{p_{\text{fin}}}{1 + e_{\text{fin}} \cos\left[\theta - (\phi_{\text{fin}} - \pi)\right]} \tag{20}$$

where the semilatus rectum and the eccentricity are

$$p_{\text{fin}} = \frac{p_0}{1 - \beta_{\min}} \tag{21}$$

$$e_{\text{fin}} = \frac{\sqrt{\mathcal{A}^2 + \mathcal{B}^2}}{1 - \beta_{\min}} \tag{22}$$

while the difference $(\phi_{\text{fin}} - \pi)$ is equal to the angle between the line of apsides and the Sun-SD line at the initial time t_0.

3.1 Generalization of the results

The previous results, obtained with $N = 1$, can be easily extended to the case of a generic number N of working cycles, see Fig. 2. The control function can now be written as the sum of N boxcar functions

$$\Delta\beta(\theta) = \Delta\beta_{\max} \sum_{i=1}^{N} \left[H(\theta - \theta_{\text{on}_i}) - H(\theta - \theta_{\text{off}_i})\right] \tag{23}$$

Exploiting the linearity of the differential equation (9), the generalization of Eq. (14) is

$$\rho(\theta) = \rho_0 \cos\theta + \rho_0' \sin\theta + \Delta\beta_{\max} \sum_{i=1}^{N} \left\{H(\theta - \theta_{\text{on}_i}) \left[1 - \cos(\theta - \theta_{\text{on}_i})\right] - H(\theta - \theta_{\text{off}_i}) \left[1 - \cos(\theta - \theta_{\text{off}_i})\right]\right\} \tag{24}$$

The polar equation of the trajectory is again in the form of Eq. (15), where $\rho(\theta)$ is given by Eq. (24). Likewise, the characteristics of the final orbit, corresponding to the SD trajectory when $\theta > \theta_{\text{off}_N}$, are easily obtained by using, again, Eqs. (16) and (19)–(22). In this case,

however, the constants $\mathcal{A}$ and $\mathcal{B}$ are given by

$$\mathcal{A} = \rho_0 - \Delta\beta_{\max} \sum_{i=1}^{N} (\cos\theta_{\mathrm{on}_i} - \cos\theta_{\mathrm{off}_i}) \tag{25}$$

$$\mathcal{B} = \rho_0' - \Delta\beta_{\max} \sum_{i=1}^{N} (\sin\theta_{\mathrm{on}_i} - \sin\theta_{\mathrm{off}_i}) \tag{26}$$

3.2 Periodic β-control

A particularly interesting scenario corresponds to a situation in which the β-control is applied at regular intervals, in such a way that $\Delta\beta$ is a periodic function of θ, until N full working cycles are completed, see Fig. 3. Such a strategy, which turns out to be useful for optimizing the semimajor axis of the osculating orbit, is referred to as "periodic β-control". Recall that, according the conventions adopted in this paper, the SD flight phase starts when the electrochromic system is turned off, i.e. with $\beta = \beta_{\min}$.

In essence, the control input $\Delta\beta = \Delta\beta(\theta)$ can be described through a square wave of finite length, equal to $2\,N\,\Delta\theta$. The variation of ρ with θ is taken from Eq. (14) by introducing the notation $(\theta_{\mathrm{on}_i} - \theta_{\mathrm{off}_i}) = \Delta\theta$, and the result is

$$\rho(\theta) = \rho_0\,\cos\theta + \rho_0'\,\sin\theta + \Delta\beta_{\max} \sum_{i=1}^{2\,N} \Big\{(-1)^{i+1}\,H(\theta - i\,\Delta\theta)\,[1 - \cos(\theta - i\,\Delta\theta)]\Big\} \tag{27}$$

Finally, the polar equation of the trajectory is again obtained from Eq. (15).

An interesting result is the expression of the final orbit tracked by the SD at the end of the N-th working cycle of the electrochromic material, that is, when $\theta > 2N\Delta\theta$ and the SD reflectivity is always equal to $\eta_{\min}$. Indeed, the right-hand side summation of Eq. (27) can be equivalently written as (Kishan, 2005)

$$\sum_{i=1}^{2\,N} \big\{(-1)^{i+1}\,H(\theta - i\,\Delta\theta)\,[1 - \cos(\theta - i\,\Delta\theta)]\big\} = \frac{\cos\left[\theta + N\,(\pi - \Delta\theta)\right]\,\sin\left[\dfrac{(2\,N+1)\,(\pi - \Delta\theta)}{2}\right]}{\sin\left(\dfrac{\pi - \Delta\theta}{2}\right)} - \cos\theta \tag{28}$$

Therefore, if $\theta > 2N\Delta\theta$

$$\rho_{\text{fin}}(\theta) = (\rho_0 - \Delta\beta_{\max})\,\cos\theta + \rho_0'\,\sin\theta + \Delta\beta_{\max}\,\frac{\cos\left[\theta + N\,(\pi - \Delta\theta)\right]\,\sin\left[\dfrac{(2\,N+1)\,(\pi-\Delta\theta)}{2}\right]}{\sin\left(\dfrac{\pi-\Delta\theta}{2}\right)} \tag{29}$$

and the trajectory equation is immediately obtained from Eq. (15).

As stated, the importance of an analytical solution for the periodic β-control case is related to a mission in which the semimajor axis of the osculating orbit is to be optimized with a locally optimal strategy. As a matter of fact, the time variation of the specific mechanical energy $\mathcal{E}$ of the osculating orbit can be written as

$$\dot{\mathcal{E}} = \boldsymbol{a}_P \cdot \boldsymbol{v} \equiv \frac{\eta\, P_\oplus\, A\, r_\oplus^2}{m\, r^3}\, \boldsymbol{r} \cdot \boldsymbol{v} \tag{30}$$

where $\boldsymbol{v}$ is the SD inertial velocity vector and $\boldsymbol{a}_P$ is the propulsive acceleration vector given by Eq. (1). At a generic Sun-SD distance r, the maximum of $\dot{\mathcal{E}}$, which coincides with the maximum time variation of the orbital semimajor axis, is obtained by varying the electrochromic reflectivity in accordance with the relation

$$\eta = \begin{cases} \eta_{\max} & \text{if} \quad \boldsymbol{r} \cdot \boldsymbol{v} \geq 0 \\ \eta_{\min} & \text{if} \quad \boldsymbol{r} \cdot \boldsymbol{v} < 0 \end{cases} \tag{31}$$

which turns into the following β-control law

$$\Delta\beta = \begin{cases} \Delta\beta_{\max} & \text{if} \quad \boldsymbol{r} \cdot \boldsymbol{v} \geq 0 \\ 0 & \text{if} \quad \boldsymbol{r} \cdot \boldsymbol{v} < 0 \end{cases} \tag{32}$$

In other terms, the maximization of the semimajor axis time-variation requires the maximum (or minimum) value of the reflectivity to be used, which implies that the electrochromic system must be turned on (or off) when the SD is moving away from (or approaching) the Sun, that is, if $\dot{r} > 0$ (or $\dot{r} < 0$). The mirror counterpart of the previous control law should instead be

used in order to minimize the time-variation of semimajor axis, which corresponds to turning the electrochromic system on when the SD is approaching the Sun. It is worth noting that, as is discussed by Quarta and Mengali (2011), the control strategy of Eq. (32), when applied to a Sun-facing photonic solar sail, is also globally (not only locally) optimal, as it maximizes the time variation of the mechanical energy in a given time interval.

To summarize, the control law of Eq. (32) states that the SD must be released at the aphelion of the parking orbit (when $\nu_0 = \pi$) and the optimal period to be taken is $\Delta\theta = \pi$, which means that the reflectivity of the electrochromic material must be changed over each angular interval of 180 degrees. Note that the final SD orbit after the last N-th working cycle can be calculated from Eq. (29) in the limit as $\pi - \theta \to 0$. The result is:

$$r_{\text{fin}}(\theta) = \frac{p_0}{1 - \beta_{\min} - (e_0 - \beta_{\min} + 2\,N\,\Delta\beta_{\max})\,\cos\theta} \tag{33}$$

which is again in the classical form of Eq. (20), with a semilatus rectum p_{fin} given by Eq. (21), an eccentricity

$$e_{\text{fin}} = \frac{e_0 - \beta_{\min} + 2\,N\,\Delta\beta_{\max}}{1 - \beta_{\min}} \tag{34}$$

and an angle $\phi_{\text{fin}} = 0$.

Note, in passing, that Eq. (34) also provides the minimum number N_{esc} of working cycles necessary to reach a condition of escape from the Sun. To this end, it simply suffices to find the least N such that the condition $e_{\text{fin}} \geq 1$ is met. Accordingly, N_{esc} is only function of $\Delta\beta_{\max}$ and e_0 through the following simple relation

$$N_{\text{esc}} = \left\lceil \frac{1 - e_0}{2\,\Delta\beta_{\max}} \right\rceil \tag{35}$$

where $\lceil \square \rceil$ is the ceil function.

3.3 Degradation Effects of the electrochromic material

An interesting issue involves the degradation effect on the reflecting film (likewise on the electrochromic material) due to a prolonged exposure of the SD to the solar radiation flux in the interplanetary space. A practical consequence of such an exposure involves a variation of the material's reflectivity, which is however quite difficult to be estimated with accuracy, being function of the reflective film's environmental history, that is, of its radiation dose. For example, as far as photonic solar sails are concerned, the radiation dose is closely related to the attitude control time history (the so called cone angle control law (McInnes, 1999)), which ultimately regulates the effective area hit by the charged particles from the Sun. An engineering analysis of the potential degradation of the reflective film material usually involves complex experimental tests. However, it is useful to obtain approximate information about the degradation effect on the spacecraft trajectory by means of simplified mathematical models. In this context, Dachwald et al. (2005, 2006, 2007) have developed semi-analytical parametric models for analyzing the behavior of photonic solar sails. The main assumption is that the generic optical coefficient of the reflective film (such as the coefficient η) has an exponential-type variation with time, and is characterized by means of suitable free parameters to be tuned as a function of the physical properties of the material in accordance with the measurements obtained by laboratory tests. Such a degradation model has been effectively used for the preliminary analysis of a solar-sail-based heliocentric mission (Dachwald et al., 2007) and, more recently, has been adopted by McInnes (2014) to obtain a closed-form analytical approximation of an interplanetary mission trajectory.

The degradation effects on the reflective film of the SD will now be evaluated by means of the simplified model discussed by McInnes (2014). Assume first that the electrochromic system is turned on along the whole interval $t - t_0 \geq 0$. At a generic time instant t the reflectivity

coefficient η is calculated with the exponentially decaying law

$$\eta = \eta_{\min} + (\eta_{\max} - \eta_{\min}) \exp\left(-\epsilon \int_{t_0}^{t} \frac{r_{\oplus}^2}{r^2}\, \mathrm{d}t\right) \tag{36}$$

where the maximum value $\eta = \eta_{\max}$ is reached at the initial time. Furthermore, ϵ is a positive parameter, related to the half-life degradation time T, defined as the time interval required to reach the mean value of η, that is

$$\epsilon \triangleq \frac{\ln 2}{T} \tag{37}$$

In other terms, when $t = T$ the value of the reflectivity coefficient is $\eta = (\eta_{\max} - \eta_{\min})/2$. For this reason T (and also ϵ) can be thought of as a performance metric (McInnes, 2014) of the electrochromic material, whose value can be obtained by experimental tests. Note that Eq. (36) is in accordance with McInnes (2014) since in this case the effective area of the SD is independent of the cone angle and is constant with time by virtue of the passive stability mechanism of the SD.

Substituting the expression of $1/r^2$ from Eq. (4) into the integral of (36) and recalling that, by assumption, $\theta = 0$ when $t = t_0$, the following result is found:

$$\eta = \eta_{\min} + (\eta_{\max} - \eta_{\min}) \exp\left(-\epsilon \int_{0}^{\theta} \frac{r_{\oplus}^2}{\sqrt{\mu_{\odot}\, p_0}}\, \mathrm{d}x\right) \tag{38}$$

which gives the value of η as a function of the polar angle

$$\eta = \eta_{\min} + (\eta_{\max} - \eta_{\min}) \exp\left(-\widetilde{\epsilon}\, \theta\right) \tag{39}$$

where $\widetilde{\epsilon}$ is the dimensionless degradation parameter defined as

$$\widetilde{\epsilon} \triangleq \frac{\epsilon\, r_{\oplus}^2}{\sqrt{\mu_{\odot}\, p_0}} \tag{40}$$

The corresponding lightness number variation with θ is obtained substituting Eq. (39) into Eq. (2), viz.

$$\beta = \beta_{\min} + (\beta_{\max} - \beta_{\min}) \exp\left(-\widetilde{\epsilon}\, \theta\right) \equiv \beta_{\min} + \Delta\beta_{\max} \exp\left(-\widetilde{\epsilon}\, \theta\right) \tag{41}$$

Now substitute Eq. (41) into (8) and take into account the transformation (6). The heliocentric dynamics of a SD with the electrochromic system always turned on is found to be described by the differential equation

$$\rho'' + \rho = \Delta\beta_{\max} \exp\left(-\widetilde{\epsilon}\,\theta\right) \tag{42}$$

with the initial conditions given by Eqs. (10) or (11). The solution of Eq. (42) is

$$\rho(\theta) = \left(\rho_0 - \frac{\Delta\beta_{\max}}{\widetilde{\epsilon}^2+1}\right)\cos\theta + \left(\rho_0' + \frac{\widetilde{\epsilon}\,\Delta\beta_{\max}}{\widetilde{\epsilon}^2+1}\right)\sin\theta + \frac{\Delta\beta_{\max}}{\widetilde{\epsilon}^2+1}\exp\left(-\widetilde{\epsilon}\,\theta\right) \tag{43}$$

and the corresponding heliocentric trajectory results

$$r(\theta) = \frac{p_0}{1-\beta_{\min} - \left(\rho_0 - \dfrac{\Delta\beta_{\max}}{\widetilde{\epsilon}^2+1}\right)\cos\theta - \left(\rho_0' + \dfrac{\widetilde{\epsilon}\,\Delta\beta_{\max}}{\widetilde{\epsilon}^2+1}\right)\sin\theta - \dfrac{\Delta\beta_{\max}}{\widetilde{\epsilon}^2+1}\exp\left(-\widetilde{\epsilon}\,\theta\right)} \tag{44}$$

Strictly speaking in this case there is not a "final" orbit tracked by the SD, as the degradation of the reflective film is a continuous phenomenon with a theoretically infinite length. However, as θ becomes sufficiently large, the exponential term in Eq. (44) becomes negligible compared to the unity and the trajectory tends (again) to a conic with equation

$$r_{\text{fin}}(\theta) = \frac{p_0}{1-\beta_{\min} - \left(\rho_0 - \dfrac{\Delta\beta_{\max}}{\widetilde{\epsilon}^2+1}\right)\cos\theta - \left(\rho_0' + \dfrac{\widetilde{\epsilon}\,\Delta\beta_{\max}}{\widetilde{\epsilon}^2+1}\right)\sin\theta} \tag{45}$$

The result obtained under the assumption of electrochromic system always turned on can also be generalized to the generic situation of N working cycles. In the latter case the control scheme in presence of degradation of the reflective film is schematically illustrated in Fig. 4. Paralleling the developments described in § 3.1, the control function can be written as

$$\Delta\beta(\theta) = \Delta\beta_{\max}\sum_{i=1}^{N}\left[\mathrm{e}^{-\widetilde{\epsilon}\theta_{\text{on}_i}}\,\mathrm{e}^{-\widetilde{\epsilon}(\theta-\theta_{\text{on}_i})}H(\theta-\theta_{\text{on}_i}) - \mathrm{e}^{-\widetilde{\epsilon}\theta_{\text{off}_i}}\,\mathrm{e}^{-\widetilde{\epsilon}(\theta-\theta_{\text{off}_i})}H(\theta-\theta_{\text{off}_i})\right] \tag{46}$$

Substituting this equation into Eq. (9) and using the Laplace transform technique, the variation of ρ with the polar angle is found to be

$$\rho(\theta) = \rho_0\cos\theta + \rho_0'\sin\theta + \frac{\Delta\beta_{\max}}{\widetilde{\epsilon}^2+1}\sum_{i=1}^{N} f_i(\theta) \tag{47}$$

where

$$
\begin{aligned}
f_i(\theta) = \quad & \mathrm{e}^{-\widetilde{\epsilon}\theta_{\mathrm{on}_i}} \left[\mathrm{e}^{-\widetilde{\epsilon}(\theta-\theta_{\mathrm{on}_i})} - \cos(\theta-\theta_{\mathrm{on}_i}) + \widetilde{\epsilon}\sin(\theta-\theta_{\mathrm{on}_i})\right] H(\theta-\theta_{\mathrm{on}_i}) \\
& - \mathrm{e}^{-\widetilde{\epsilon}\theta_{\mathrm{off}_i}} \left[\mathrm{e}^{-\widetilde{\epsilon}(\theta-\theta_{\mathrm{off}_i})} - \cos(\theta-\theta_{\mathrm{off}_i}) + \widetilde{\epsilon}\sin(\theta-\theta_{\mathrm{off}_i})\right] H(\theta-\theta_{\mathrm{off}_i})
\end{aligned}
\tag{48}
$$

4 Case study

The previously described mathematical model is now used to find the heliocentric SD trajectory for some mission scenarios. The correctness of the model has been preliminarily assessed by checking the coincidence of the trajectories obtained with the analytical model and those found by numerically integrating the equations of motion. In the latter case, the differential equations have been integrated in double precision using a variable order Adams-Bashforth-Moulton solver scheme (Shampine and Gordon, 1975; Shampine and Reichelt, 1997) with absolute and relative errors of 10^{-12}.

Three different SD configurations have been investigated whose main characteristics, taken from Colombo and McInnes (2011), are summarized in Tab. 1. They are representative of a SD of low (SD_1), medium (SD_2), and high (SD_3) performance. The approximate dimensions of these devices can be estimated by using the square configuration with a side length of $\ell = 10\,\mathrm{mm}$, as suggested by Atchison and Peck (2010). Following the analysis of Lücking et al. (2012), the coating film thickness of SD_1 is slightly less than $0.02\,\mathrm{mm}$, that of SD_2 is $0.02\,\mathrm{mm}$, and that of SD_3 is about $0.006\,\mathrm{mm}$. In all of the three cases the minimum value of the reflectivity coefficient is assumed to be $\eta_{\min} = 1$, which corresponds to a complete absorption of the impinging photons, and the maximum reflectivity coefficient is $\eta_{\max} = 1.8$, thus implying a non-specular reflection. Note that $\eta_{\max} = 1.8$ is a typical value for a photonic solar sail under the assumption of an optical thrust model (McInnes, 1999; Mengali and Quarta, 2005). For the sake of completeness Table 1 also reports the minimum and maximum value of the attainable

characteristic acceleration a_c. The latter, in analogy with a photonic solar sail, is defined as the modulus of the propulsive acceleration due to the solar radiation pressure at a distance from the Sun equal to $r = r_\oplus$.

To simplify the following discussion, assume a single working cycle of the electrochromic material, i.e. $N = 1$. The aim of this choice is to validate the analytical model by means of a simple mission case. Such a choice, however, is consistent with a potential application of a SD spacecraft. A more involved control strategy (such as a situation where the electrochromic system is switched on or off several times) can be applied to a mission scenario involving the maximization (or minimization) of the semimajor axis of the osculating orbit. In the latter case, a multiple application of the analytical relations described in this paper allows the characteristics of the orbits tracked by the SD to be easily calculated .

Assume, therefore, that $N = 1$. The initial parking orbit coincides with the heliocentric Earth's orbit, with $e_0 = 0.01671$ and a semimajor axis equal to 1 au (therefore $p_0 = 0.99972$ au). This choice corresponds to a situation in which the container of all SDs is released on a parabolic orbit with respect to the Earth. Each SD therefore tracks the same heliocentric orbit of Earth after the escape phase. To reduce the number of free parameters, the initial SD position is assumed to coincide with the perihelion of the parking orbit, that is, $\nu_0 = 0$. The degradation effect is also neglected. The SD trajectory can be therefore calculated by means of Eqs. (15) and (16), which, of course, depend on the value of the polar angle when the electrochromic system is turned on (at $\theta = \theta_{\rm on}$) and off ($\theta = \theta_{\rm off}$).

The results are obtained parametrically as a function of these two angles, where $\theta_{\rm on} \in [0,\, 360]$ deg and $\theta_{\rm off} = \theta_{\rm on} + \Delta\theta$, with $\Delta\theta \in [0,\, 360]$ deg. The corresponding isocontour lines are shown in Figs. 5–7 for the three previous SD configurations. These figures illustrate the variation of the ratio of the final orbit to the parking orbit eccentricity ($e_{\rm fin}/e_0$), as a function of the pair $\{\theta_{\rm on}, \Delta\theta\}$. The isocontour lines of the surface $e_{\rm fin} = e_{\rm fin}(\theta_{\rm on}, \Delta\theta)$ are split into two sub-figures

to make the visualization easier. The same Figs. 5–7 can also be used to find the value of the semimajor axis of the final orbit as a function of the pair $\{\theta_{\rm on}, \Delta\theta\}$. This is possible through Eq.(21), whose value is independent of the electrochromic material. The results are $p_{\rm fin} = 1.013271\,{\rm au}$ for SD_1, $p_{\rm fin} = 1.025433\,{\rm au}$ for SD_2, and $p_{\rm fin} = 1.043564\,{\rm au}$ for SD_3.

The Figs. 5–7 present common features. For example, for a given value of $\Delta\theta$, that is, for a given angular interval in which the electrochromic material is turned on, the final eccentricity is a periodic function of $\theta_{\rm on}$. A special case corresponds to $\Delta\theta = 360\,{\rm deg}$, i.e. when the electrochromic material operates for a full revolution around the Sun. In that case, the eccentricity of the final orbit takes a constant value independent of $\theta_{\rm on}$. This value coincides with the eccentricity that would be obtained by releasing the SD at a point with an anomaly $\theta_{\rm on}$ and subsequently by maintaining the electrochromic system off. Note that Eq. (22) provides

$$e_{\rm fin} = \frac{\sqrt{\rho_0^2 + (\rho_0')^2}}{1 - \beta_{\rm min}} \equiv \frac{\beta_{\rm min} + e_0}{1 - \beta_{\rm min}} \tag{49}$$

In the examined cases, a nearly circular orbit can be obtained (within a single working cycle) by means of a high-performance SD only, that is, using the SD_3 configuration. As a matter of fact, from Fig. 7 the condition $e_{\rm fin} = 0$ can be obtained by selecting $\theta_{\rm on} = 210\,{\rm deg}$ and $\Delta\theta = 120\,{\rm deg}$, or $\theta_{\rm on} = 150\,{\rm deg}$ and $\Delta\theta = 240\,{\rm deg}$. In both cases $e_{\rm fin}$ is smaller than $0.03\,e_0$.

Finally, Figs. 5–7 show that the maximum value of the eccentricity (and of the semimajor axis) of the final orbit is reached when $\theta_{\rm on} = 0\,{\rm deg}$ and $\Delta\theta = 180\,{\rm deg}$. This corresponds to switching the electrochromic system on at the perihelion of the parking orbit and switching it off at the aphelion. This strategy is in agreement with the previous analysis about the periodic β-control, in which the importance of the case $\Delta\theta = 180\,{\rm deg}$ has been emphasized. In the latter case the maximum value of the final eccentricity is again obtained from Eq. (22) by observing

that $\mathcal{A} = -(e_0 + \beta_{\min} + 2\,\Delta\beta_{\max})$ and $\mathcal{B} = 0$, see Eqs. (17) and (18). Therefore

$$\max(e_{\text{fin}}) = \frac{e_0 + \beta_{\min} + 2\,\Delta\beta_{\max}}{1 - \beta_{\min}} \tag{50}$$

Note that Eq. (50) cannot be obtained directly from Eq. (34) with $N = 1$. Indeed, Eq. (34) implies that $\nu_0 = \pi$, since the periodic β-control assumes that the electrochromic system at the starting position is switched off.

5 Conclusions

The dynamics of a smart dust with electrochromic material has been studied under the effect of a β-control strategy, in which the force due to the solar radiation pressure is modulated between two values by changing the reflectivity of the coating film. The problem has been addressed assuming that the smart dust is passively Sun-pointing, which implies that the propulsive acceleration is always in the radial (outward) direction and the resulting spacecraft motion is two-dimensional. The spacecraft dynamics has been conveniently transformed using a Bürdet-Ferrándiz regularization, which allows the Sun-spacecraft dimensionless distance to be described by the differential equation of a single degree of freedom linear harmonic oscillator with unitary frequency, whose forcing input is a boxcar function. In this new form the problem can be solved using the Laplace transform theory and a closed form solution of the trajectory has been obtained. Depending on the period of exposition to the solar radiation (including particle radiation), the coating film reflectivity is known to decay with time. This phenomenon is modelled by assuming that the reflectivity coefficient reduces according to an exponential law of variation. Notably, the smart-dust trajectory can be found as a generalization of the previous result where no degradation effect was accounted for.

The effectiveness of a smart-dust concept is mainly associated to the very high area-to-mass ratios of these devices, which allows the thrust obtained from the differential use of the solar

radiation pressure (i.e. by switching the electrochromic material either off or on) to produce an high value of characteristic acceleration. Three cases of smart-dust configurations have been analyzed, being representative of spacecraft with low, medium and high performance. The simulation results show that with a single variation of the reflectivity coefficient the final orbit eccentricity can be increased up to three times its initial value for a low performance smart dust and up to eight times its initial value for a spacecraft of high performance. In this last case it is also possible to circularize the orbit by suitably selecting the maneuver point.

As a matter of fact, using the current technology level, the more suitable scenario for a micro spacecraft (and also for a smart dust) is a planetary mission, that is, a scenario in which the distance between the space vehicles and the Earth is within the (reduced) transmission capabilities of these advanced (and to some extent "exotic") devices. Anyway, the main aim of this work is to emphasize the possibility of obtaining the deep space trajectory of a smart dust in closed form. The availability of a new set of analytical equations for the trajectory analysis is an important starting point for promoting the research of new heliocentric mission applications.

In this context, a possible extension of this work involves the study of a discrete variation of the β-control, which includes more than two thrust levels. This happens when the electrochromic film is made of micro-cells (or micro-panels) that can be operated independently one from another.

References

Aliasi, G., Mengali, G., Quarta, A. A., Passive control feasibility of collinear equilibrium points with solar balloons. J. Guid. Control. Dynam. 35 (5), 1657–1661, doi: 10.2514/1.57393, September-October 2012.

Aliasi, G., Mengali, G., Quarta, A. A., Artificial lagrange points for solar sail with

electrochromic material panels. J. Guid. Control. Dynam. 36 (5), 1544–1550, doi: 10.2514/1.58167, September-October 2013.

Aliasi, G., Mengali, G., Quarta, A. A., Artificial equilibrium points for a solar balloon in the alpha centauri system. Acta Astronaut. 104 (2), 464–471, doi: 10.1016/j.actaastro.2014.03.006, November-December 2014.

Atchison, J. A., Peck, M. A., A passive, sun-pointing, millimeter-scale solar sail. Acta Astronaut. 67 (1-2), 108–121, doi: 10.1016/j.actaastro.2009.12.008, July-August 2010.

Biggs, J. D., McInnes, C. R., Passive orbit control for space-based geo-engineering. J. Guid. Control. Dynam. 33 (3), 1017–1020, doi: 10.2514/3.21211, May-June 2010.

Bürdet, C. A., Le mouvement Keplerien et les oscillateurs harmoniques. J. Reine Angew. Math. 1969 (238), 71–84, doi: 10.1515/crll.1969.238.71, January 1969.

Colombo, C., Lücking, C., McInnes, C. R., Orbital dynamics of high area-to-mass ratio spacecraft with J_2 and solar radiation pressure for novel Earth observation and communication services. Acta Astronaut. 81, 137—50, doi: 10.1016/j.actaastro.2012.07.009, 2012.

Colombo, C., Lücking, C., McInnes, C. R., Orbit evolution, maintenance and disposal of spacechip swarms through electro-chromic control. Acta Astronaut. 82 (1), 25–37, doi: 10.1016/j.actaastro.2012.05.035, 2013.

Colombo, C., McInnes, C. R., Orbital dynamics of "Smart-Dust" devices with solar radiation pressure and drag. J. Guid. Control. Dynam. 34 (6), 1613–1631, doi: 10.2514/1.52140, 2011.

Colombo, C., McInnes, C. R., Orbit design for future spacechip swarm missions in a planetary atmosphere. Acta Astronaut. 75, 25–41, doi: 10.1016/j.actaastro.2012.01.004, 2012.

Dachwald, B., Macdonald, M., McInnes, C. R., et al., Impact of optical degradation on solar sail mission performance. J. Spacecraft Rockets 44 (4), 740–749, doi: 10.2514/1.21432, July-August 2007.

Dachwald, B., Mengali, G., Quarta, A. A., et al., Parametric model and optimal control of solar sails with optical degradation. J. Guid. Control. Dynam. 29 (5), 1170–1178, doi: 10.2514/1.20313, September-October 2006.

Dachwald, B., Seboldt, W., Macdonald, M., et al., Potential solar sail degradation effects on trajectory and attitude control. In: AIAA Guidance, Navigation, and Control Conference and Exhibit. San Francisco, USA, paper AIAA 2005-6172, 15–18 August 2005.

Ferrándiz, J. M., A general canonical transformation increasing the number of variables with application to the two-body problem. Celest. Mech. Dyn. Astr. 41 (1–4), 343–357, doi: 10.1007/BF01238770, March 1987.

Fukushima, T., New two-body regularization. Astron. J. 133 (1), 1–10, doi: 10.1086/509606, January 2007.

Gong, S., Li, J., Solar sail halo orbit control using reflectivity control devices. T. Jpn. Soc. Aeronaut. S. 57 (5), 279–288, doi: 10.2322/tjsass.57.279, 2014a.

Gong, S., Li, J., Solar sail heliocentric elliptic displaced orbits. J. Guid. Control. Dynam. 37 (6), 2021–2025, doi: 10.2514/1.G000660, November-December 2014b.

Gong, S., Li, J., Equilibria near asteroids for solar sails with reflection control devices. Astrophys. Space Sci. 355 (2), 213–223, doi: 10.1007/s10509-014-2165-7, 2015.

Kishan, H., Trigonometry. Atlantic Publishers and Distributors, New Delhi, Ch. 9, pp. 216–218, ISBN: 81-269-0560-3, 2005.

Lücking, C., Colombo, C., McInnes, C. R., Electrochromic orbit control for smart-dust devices. J. Guid. Control. Dynam. 35 (5), 1548–1558, doi: 10.2514/1.55488, 2012.

Lücking, C. M., Colombo, C., McInnes, C. R., Orbit control of high area-to-mass ratio spacecraft using electrochromic coating. In: 61st International Astronautical Congress. Also paper IAC-10-C1.2.7, 2010.

McInnes, C. R., Solar Sailing: Technology, Dynamics and Mission Applications. Springer-Praxis Series in Space Science and Technology. Springer-Verlag, Berlin, pp. 13–14, 46–54, 1999.

McInnes, C. R., Orbits in a generalized two-body problem. J. Guid. Control. Dynam. 26 (5), 743–749, doi: 10.2514/2.5129, September-October 2003.

McInnes, C. R., Approximate closed-form solution for solar sail spiral trajectories with sail degradation. J. Guid. Control. Dynam. 37 (6), 2053–2057, doi: 10.2514/1.G000225,

November-December 2014.

Mengali, G., Quarta, A. A., Optimal three-dimensional interplanetary rendezvous using non-ideal solar sail. J. Guid. Control. Dynam. 28 (1), 173–177, doi: 10.2514/1.8325, January-February 2005.

Mu, J., Gong, S., Li, J., Coupled control of reflectivity modulated solar sail for geosail formation flying. J. Guid. Control. Dynam. 38 (4), 740–751, doi: 10.2514/1.G000117, April 2015.

Quarta, A. A., Mengali, G., Optimal switching strategy for radially accelerated trajectories. Celest. Mech. Dyn. Astr. 105 (4), 361–377, doi: 10.1007/s10569-009-9233-2, December 2009.

Quarta, A. A., Mengali, G., Linear systems approach to multiple-impulse trajectory analysis via regularization. J. Guid. Control. Dynam. 33 (5), 1679–1683, doi: 10.2514/1.50133, September-October 2010.

Quarta, A. A., Mengali, G., Analytical results for solar sail optimal missions with modulated radial thrust. Celest. Mech. Dyn. Astr. 109 (2), 147–166, doi: 10.1007/s10569-010-9319-x, February 2011.

Quarta, A. A., Mengali, G., New look to the constant radial acceleration problem. J. Guid. Control. Dynam. 35 (3), 919–929, doi: 10.2514/1.54837, May-June 2012.

Quarta, A. A., Mengali, G., Analysis of electric sail heliocentric motion under radial thrust. J. Guid. Control. Dynam. In press, doi: 10.2514/1.G001632, 2015.

Shampine, L. F., Gordon, M. K., Computer Solution of Ordinary Differential Equations: The Initial Value Problem. W. H. Freeman, San Francisco, Ch. 10, 1975.

Shampine, L. F., Reichelt, M. W., The MATLAB ODE suite. SIAM J. Scient. Comp. 18 (1), 1–22, doi: 10.1137/S1064827594276424, January 1997.

Yamakawa, H., Optimal radially accelerated interplanetary trajectories. J. Spacecraft Rockets 43 (1), 116–120, doi: 10.2514/1.13317, January–February 2006.

List of Tables

1 Representative smart-dust characteristics with $\eta_{\min} = 1$ and $\eta_{\max} = 1.8$. Data adapted from Colombo and McInnes (2011). 28

name	SD_1	SD_2	SD_3
A/m [m^2/kg]	17.3913	32.6087	54.6364
$a_{c_{min}}$ [mm/s^2]	0.0793	0.1487	0.2491
$a_{c_{max}}$ [mm/s^2]	0.1427	0.2677	0.4485
β_{min}	0.0134	0.0251	0.0420
β_{max}	0.0241	0.0451	0.0756
$\Delta\beta_{min}$	0.0107	0.0201	0.0336

Table 1
Representative smart-dust characteristics with $\eta_{min} = 1$ and $\eta_{max} = 1.8$. Data adapted from Colombo and McInnes (2011).

List of Figures

1	Reference frame.	30
2	Schematic representation of the control input.	31
3	Scheme of the periodic β-control.	32
4	Schematic representation of the control input in presence of exponential degradation.	33
5	Final orbit's eccentricity as a function of $\{\theta_{\text{on}}, \Delta\theta\}$ for a low-performance smart dust (SD_1) with a single electrochromic control activation ($N = 1$).	34
6	Final orbit's eccentricity as a function of $\{\theta_{\text{on}}, \Delta\theta\}$ for a medium-performance smart dust (SD_2) with a single electrochromic control activation ($N = 1$).	35
7	Final orbit's eccentricity as a function of $\{\theta_{\text{on}}, \Delta\theta\}$ for a high-performance smart dust (SD_3) with a single electrochromic control activation ($N = 1$).	36

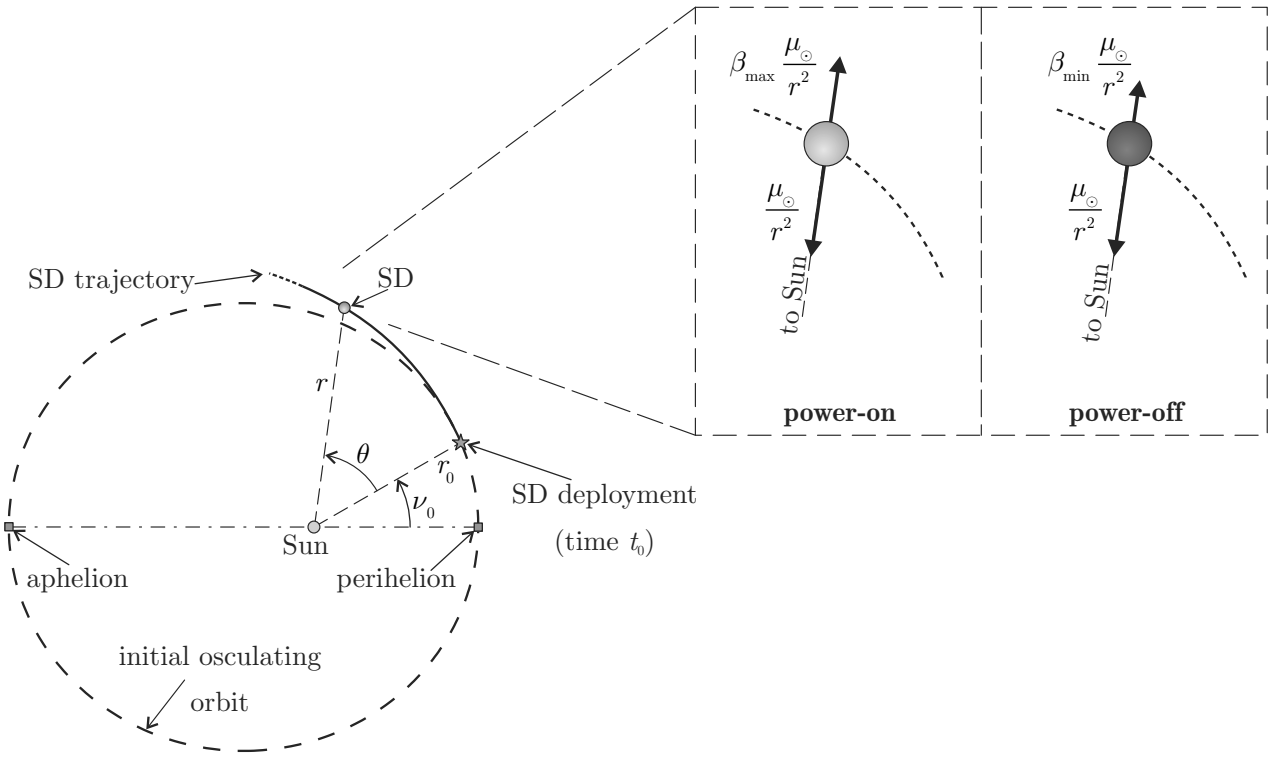

Fig. 1. Reference frame.

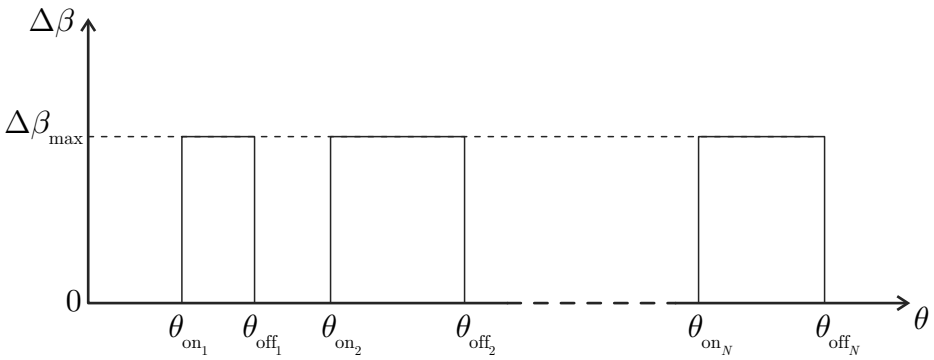

Fig. 2. Schematic representation of the control input.

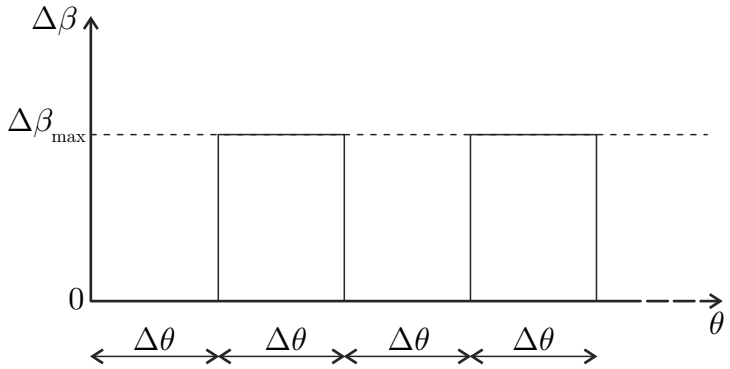

Fig. 3. Scheme of the periodic β-control.

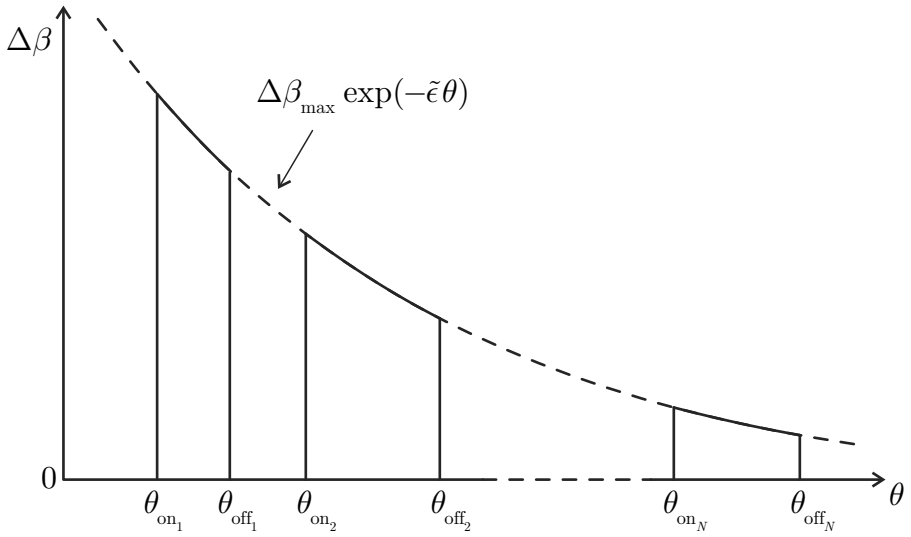

Fig. 4. Schematic representation of the control input in presence of exponential degradation.

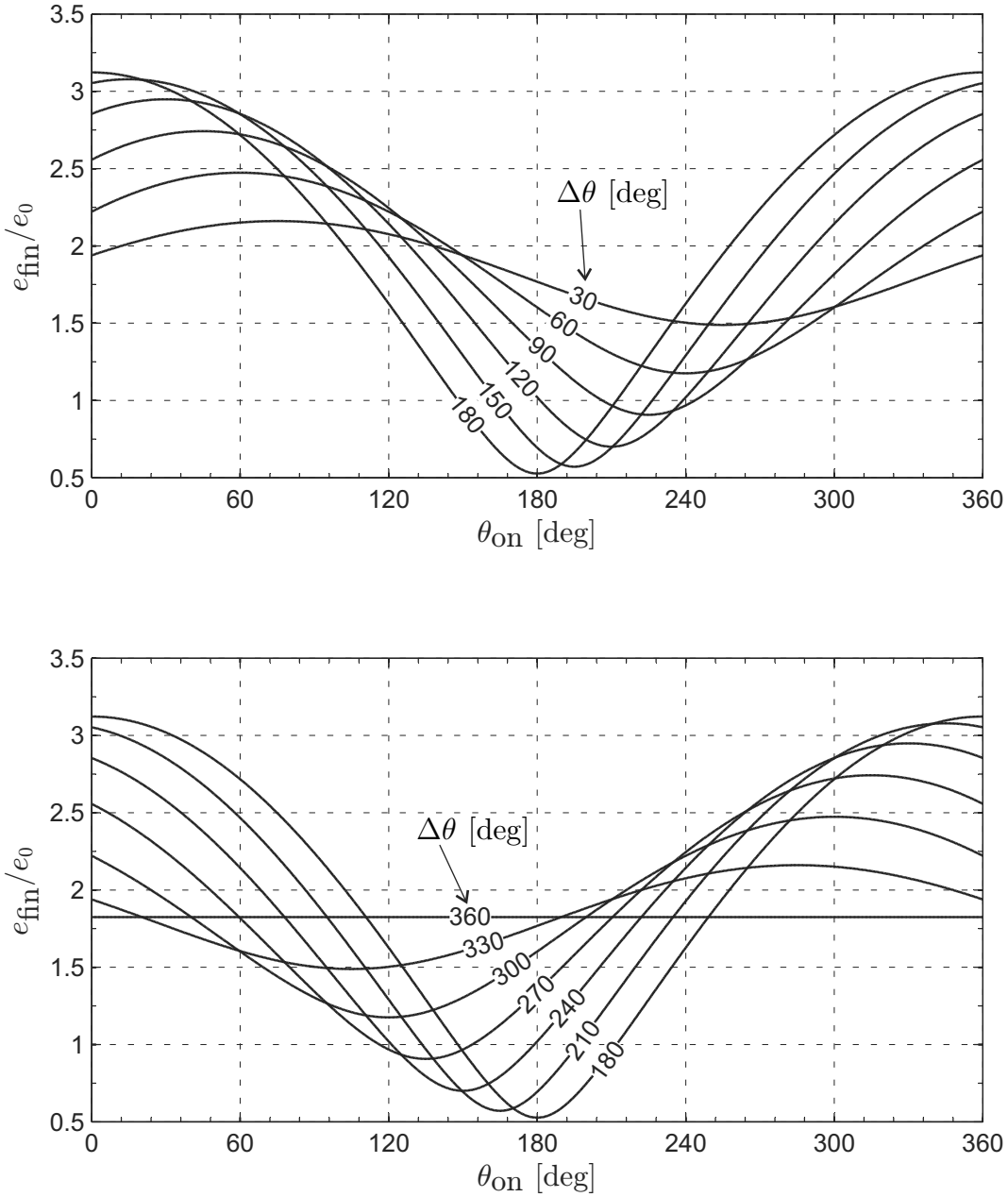

Fig. 5. Final orbit's eccentricity as a function of $\{\theta_{\rm on}, \Delta\theta\}$ for a low-performance smart dust (SD_1) with a single electrochromic control activation ($N = 1$).

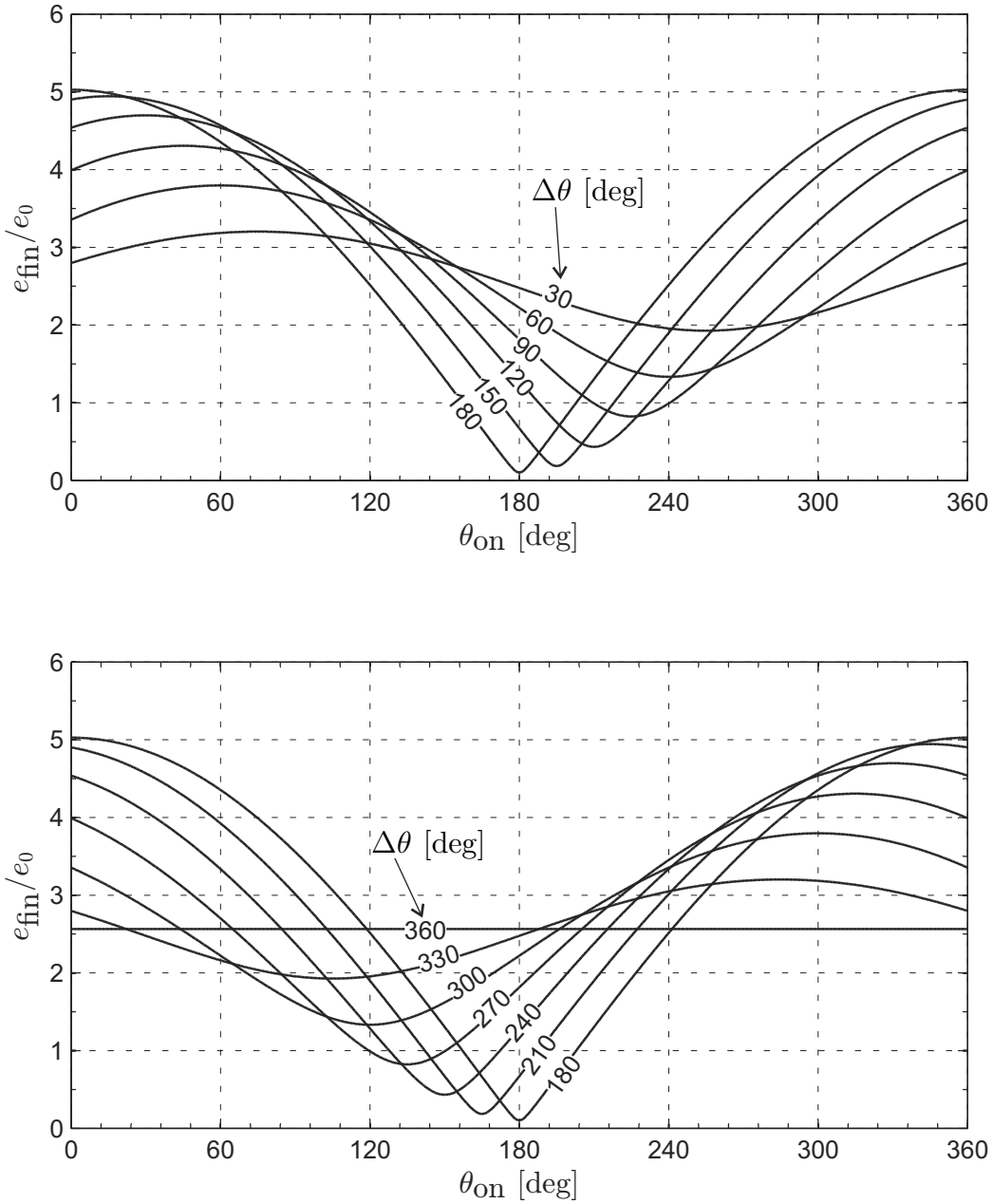

Fig. 6. Final orbit's eccentricity as a function of $\{\theta_{\rm on}, \Delta\theta\}$ for a medium-performance smart dust (SD_2) with a single electrochromic control activation ($N = 1$).

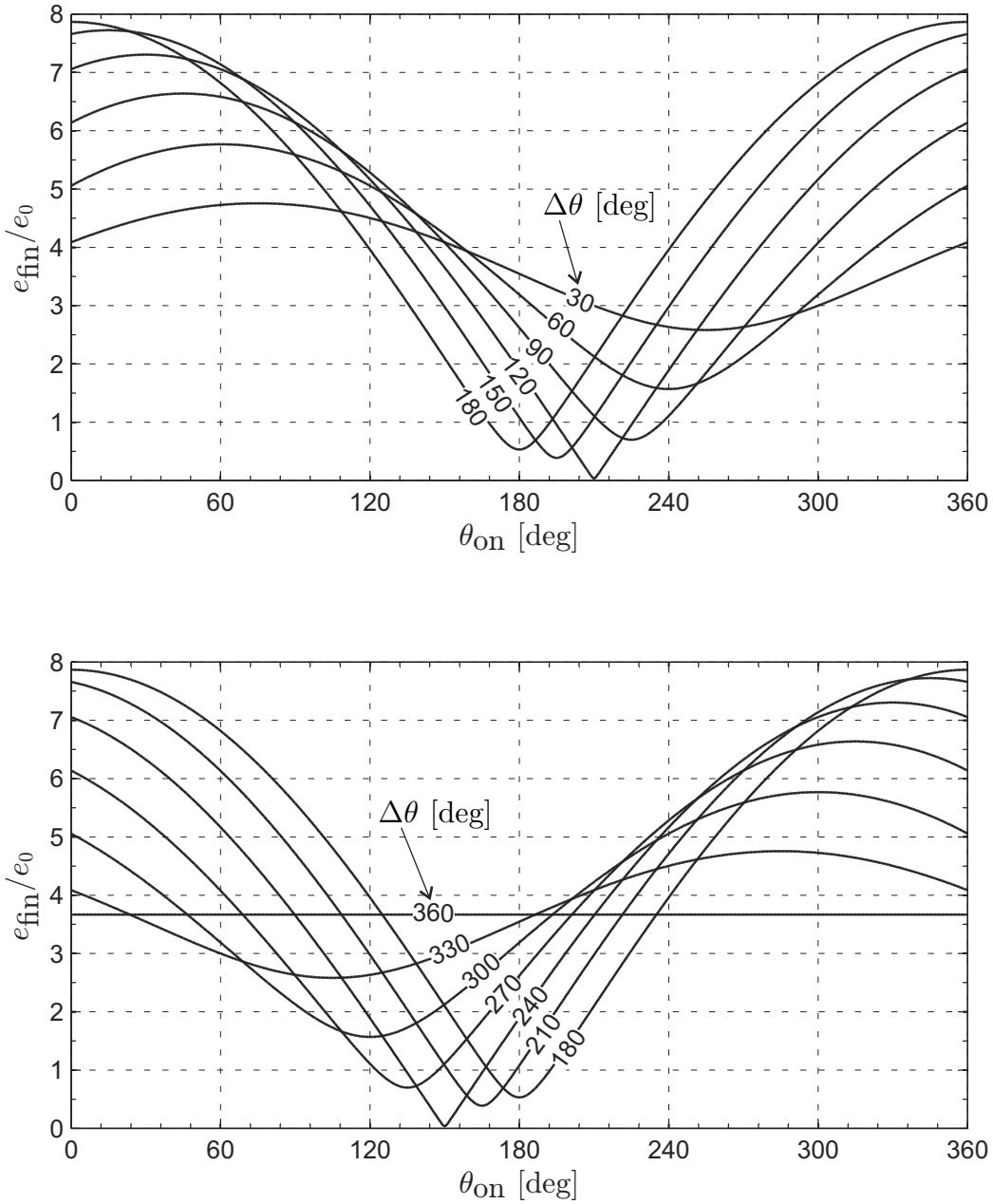

Fig. 7. Final orbit's eccentricity as a function of $\{\theta_{\rm on}, \Delta\theta\}$ for a high-performance smart dust (SD_3) with a single electrochromic control activation ($N = 1$).